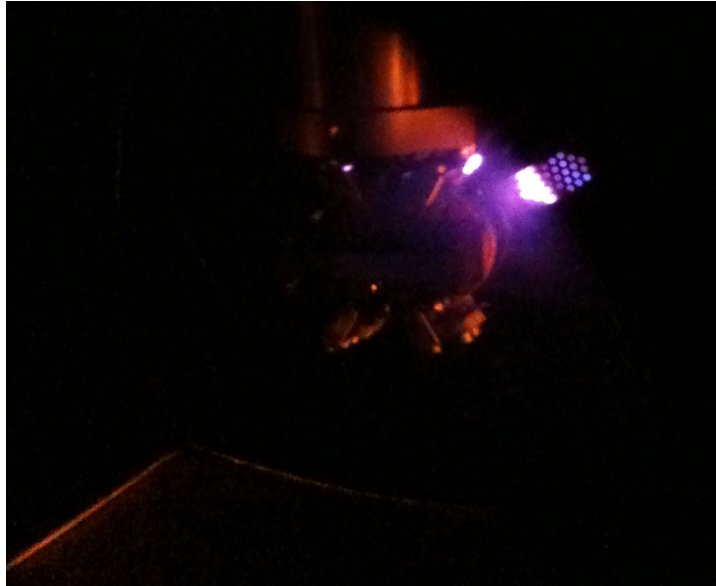


University of Twente

Relation between Surface Roughness and Adhesion as studied with AFM



Author: John Kostakos
Supervisors: Professor Dr. Ir. Harold Zandvliet
Dr. Ir. Herbert Wormeester
Dr. Arzu Colak

**Physics of Interfaces and Nanomaterials
Faculty of Science and Technology
MESA+ Institute of Technology**

December 2013

Relation between Surface Roughness and Adhesion as studied with AFM

By: John Kostakos

A thesis submitted in fulfillment of the requirements for the degree of Master of
Science, Applied Physics

December 2013

Exam committee:

Prof. Dr. Ir. H. J. W. Zandvliet

Dr. Ir. H. Wormeester

Dr. Ir. Annemarie Huijser

This work was performed at:

Physics of Interfaces and Nanomaterials MESA+ Institute for Nanotechnology
University of Twente P.O. Box 217 7500 AE Enschede

It doesn't matter how beautiful your theory is, it doesn't matter how smart you are.
If it doesn't agree with experiment, it's wrong.

Richard P. Feynman

Image on cover: Grid of the ion source that produces Ar^+ . The purple color is the ions color. With orange color is depicted the sample holder that keeps the CrN sample in normal incidence position.

Abstract

The surface roughness and adhesion for Chromium Nitride samples are studied with Atomic Force Microscopy. The CrN samples were sputtered by Ion Bombardment with 1.5 keV Ar⁺ in normal incidence for different time sputtering. The morphology change is determined in terms of RMS roughness and Adhesion force. In addition Contact Angle and Four Probe Surface Resistance measurements were performed in all samples. As a reference an unsputtered sample was used and a polished flat CrN sample as well.

From the surface statistics we observed a surface smoothing for the first 20 minutes of sputtering and a surface roughening from 30 to 60 minutes. The adhesion force was measured using force-distance measurement revealing an inversely proportional relation to the roughness values as predicted by the theory [1]. From the contact angle experiment the hydrophobicity of the surface was determined. The surface sheet resistance is increasing proportionally to the sputtering times as revealed from the four probe resistivity measurements.

Contents	
<u>Introduction</u>	7
<u>Brief Theory</u>	8
Materials.....	8
Ion Beam Bombardment	8
Sputtering	9
Atomic Force Microscopy.....	10
1 st Order Statistics	10
2 nd Order Statistics	12
Adhesion.....	14
Surface Forces	14
Adhesion measurement with AFM.....	16
Instrumentation: How to convert Voltage to Force measurement	17
Contact Angle.....	18
Resistivity	19
<u>Experimental Set-Up and Methods</u>	21
Sample Preparation	21
System Description.....	21
Ion Bombardment	22
Atomic Force Microscopy.....	23
Topography imaging	24
From a measured topography to statistical quantities	25
Force-Distance Measurements	25
Contact Angle Measurements.....	28
Four Probe Resistance Measurements.....	29
<u>Results and Discussion</u>	32
Morphology	32
AFM Images.....	32
1 st Order Statistics	33
2 nd Order Statistics	35
AFM Force-Distance Measurements	37
Contact Angle Measurements.....	39
Four Probe Resistance Measurements.....	41
<u>Conclusions and Future Perspectives</u>	42
<u>Acknowledgments</u>	43
<u>Bibliography</u>	44

Introduction

In the recent decades a drive for smaller and more efficient devices was pushed by technological possibilities and consumer wishes. This is only possible with a combination of pushing current technology to its limits and scientific research for creating new technological opportunities. Currently one of the biggest markets is this of the chip industry. This type of industry keeps growing with a gigantic rhythm for over 50 years. The main demand is the reduction in size and cost of the chips that assembly the new technological devices. The production line of chips manufacturing consists of different and multitasking procedure that the Si wafers should go through. The necessity for a better handling and moving of the wafers through different positions during the chip production line indicates the need for a wafer tray on which the increasingly large but delicate wafers are placed on. The manufacturing process involves a lithography step that requires a positional fixation on a nm scale. In addition to sufficient friction a low adhesion is required. These requirements are very often contradictory. Surface science can help to find solutions for these industrial requirements.

In order to achieve these surface characteristics we used a material that is beneficial for industrial usage, Chromium Nitride (CrN). It has a good corrosion resistance, is cheap to produce and is often used for coating of industrial equipment. The adhesion properties of the CrN surface are tried to manipulate in this study by changing the morphology via ion sputtering. The main parameters that determine the sputtering process are the energy of the ions (1.5 keV in this study), the polar angle of incidence for sputtering (normal incidence sputtering in this study) and the ion current and sputter time. The latter was varied between 5 and 60 minutes. With Atomic Force Microscopy (AFM), the topography was imaged in the relevant length scale between 5 nm and 20 μm . The adhesion was also measured with AFM from force distance spectroscopy with a flat tip with a 2 μm diameter. In addition we performed contact angle measurements in order to verify whether sputtering altered the surface energetics. Four probe resistivity measurements were performed as a fast characterization method for sputter influence.

The organization of this essay is built in order to cover the requirements for a MSc thesis. First we give a brief theory of the background physics that are used in this study. Then we give a description of the experimental equipment and the methods that we use. Next is the chapter that includes the experimental results and their interpretation. The conclusions and future perspectives are concluding the thesis followed by the acknowledgments and bibliography

Brief Theory

Materials

Chromium can combine with Nitrogen in order to form a stable stoichiometric metal nitride compound named Chromium Nitride, CrN. In this study we investigate the surface properties evolution of CrN samples as a function of roughness. CrN is a transition metal nitride with high thermal stability, non corrosive and with excellent mechanical properties [2]. It has a cubic structure with lattice constant equal to 4.14 Angstroms [3].

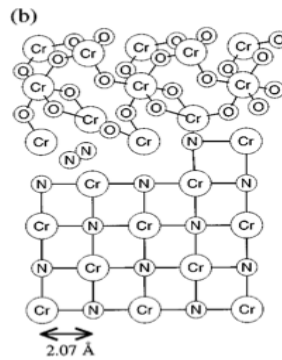


Figure 1: CrN Oxidized and bulk structure [3].

CrN is an interstitial compound. Chromium has a body-centered cubic crystal structure. Nitrogen has a smaller atomic radius and occupies the interstitial 'holes' of the octahedral Chromium lattice [4]. It has a salt rock structure.

Ion Beam Bombardment

Sputtering occurs when atoms are removed from a solid surface as a result of the surface bombardment with accelerated ions. This technique established by W. R. Grove in 1852[5]. In literature this method is referred to with different names as: ion beam deposition, ion bombardment, physical vapor deposition, ion deposition, ion erosion, physical vapor sputtering, ion sputtering etc. In this study we mention this technique as sputtering or ion beam bombardment.

We introduce Ar in a vacuum chamber. Electrons are generated that collide with the Ar atoms. We use Ar because in an inert-noble gas with mass range similar to this of Cr in order to be able to remove Cr atoms. The collision between electrons and Ar atoms creates Argon ions i.e. Ar⁺. With an additional voltage the ions are accelerated [6]. We will try to explain briefly the main aspects of physics behind this experimental method.

Sputtering

The bombardment of solid surface targets with ions results in different processes such as: ion backscattering, ion implantation and electrons emission. In average a metallic bond in the CrN surface has an energy range of a few eV [7]. Thus a collision of a metallic surface with an Ar⁺ with an average energy of 1.5 keV causes a variety of physical phenomena at the surface and for the first layers of the material sample, such as atomic displacement resulting lattice defects in terms of vacancies and interstitials. The ions transfer part of their momentum to the surface atoms. Consequently the surface atoms receive enough kinetic energy in order to create further collisions with other surface atoms and hence further atoms displaced. These phenomena are depended on the transferred energy. Thus sputtering can cause a situation named collision cascade [8]. Momentum reversal causes the surface atoms, after the ions collision, to move towards the surface and, in the case of gaining enough kinetic energy from the incident ions, these surface atoms can overcome the surface binding energy barrier. As a result these atoms are ejected from the surface and the continuous sputtering can cause surface erosion in terms of defects in crystalline structure leading to an amorphous surface.

In this work we perform low energy sputtering, which means ion energy less than 2 keV. In the low energy range the ions loose their energy in an elastic way and the collision phenomena are restricted only at the near surface region [9]. The main parameters that determine sputtering are: the ion flux, which is the amount of ions per area hitting the surface, the ion fluence, which is the amount of current that flows per area hitting the surface, the angle of incidence, which in our case is normal i.e. zero degrees, and the time of sputtering that every sample receives.

The morphology of the surface changes due to sputtering causing roughness or smoothness of the surface. These phenomena can be explained as a competition of different kinetic processes that activated due to ion bombardment. The sputter removal causes the roughening of the surface while the surface diffusion of point defects causes the smoothening of the surface [10].

By changing the parameters that determine sputtering (time, flux in terms of ions energy, angle of incidence etc) we get roughening or smoothness of our surfaces. Thus we can examine our surface in the micro-scale in terms of mounds or vacancy islands. In order to study our surface in this detail we make use of Atomic Force Microscopy.

Atomic Force Microscopy

The surface topography studies require an experimental method that ensures high resolution and good statistics. A technique that meets these requirements is Atomic Force Microscopy (AFM)[11]. In general there are three AFM modes: the contact mode, the tapping or intermittent mode and the non-contact mode. In our study we make use of the tapping mode in order to achieve high-resolution images while reducing the lateral forces.

A cantilever is mounted at a piezoelectric transducer chip. This piezo vibrates and cause the tip to oscillate. A laser spot that is positioned on the backside of the tip is reflected towards a photo-detector that transforms the oscillation of the cantilever to a voltage. The tip is oscillated near its resonant frequency while keeping the oscillation amplitude constant using a feedback loop as the tip scans over the surface. The feed back loop regulates the height of the cantilever with respect to the surface using a z-piezo.

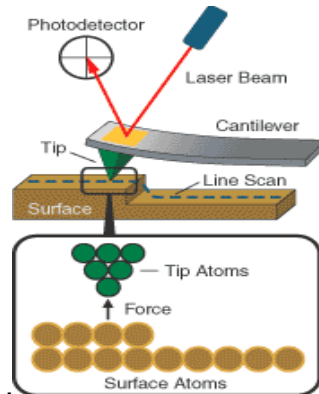


Figure 2: AFM scanning procedure [image taken by www.agilent.com].

During the approach of the tip near the surface due to tip-sample interaction the resonance frequency shifts i.e. for attractive forces the frequency is reduced while for repulsive forces is increased [1]. In the high amplitude state of the tip called the repulsive state while the low amplitude is called the attractive state [12]. Thus we get the space information for height as a function of x and y values i.e. $h(x,y)$. From this information we can calculate surface statistics parameters by using the mathematical models that describe these.

1st Order Statistics

A very useful tool for morphology characterization is to look at statistical averages. The 1st order statistical quantities. In first order statistics the height distribution is considered. In this essay the height variations of a surface are depicted in a histogram of a distribution $p(h)$ of occurring heights h like this in figure [down]. these histograms are normalized in such a way that:

$$\int_{-\infty}^{+\infty} p(h)dh = 1$$

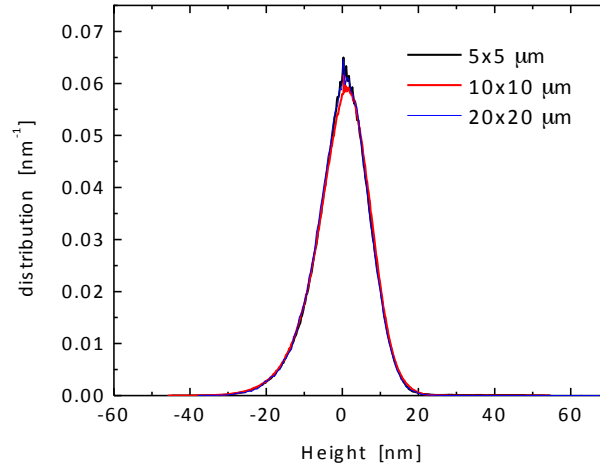


Figure 3 Histogram of a CrN surface for three different AFM measurements.

The height variation can be expressed with a series of values, the so called moments m_n defined as:

$$m_n = \int_{-\infty}^{\infty} p(h)h^n dh$$

Because usually at most only the first four moments are calculated, they have their own specific names:

1. m_1 is the mean value, which has to be zero as a result of the background subtraction procedure used. Its numerical estimation for a surface length N is

$$\langle h \rangle = \frac{1}{N} \sum_{i=1}^N h_i$$

2. m_2 is the variance of the surface height. The root mean square roughness, or rms roughness, of a surface is defined as $w = \sqrt{m_2}$ and its numerical estimation for an N surface length is

$$\langle w \rangle = \left\{ \frac{1}{N} \sum_{i=1}^N [h_i - \langle h \rangle]^2 \right\}^{1/2}$$

3. m_3 is used to calculate the skewness, which is $\left(\frac{m_3}{m_2^{3/2}}\right)$. The division makes that the skewness is a normalized dimensionless value. A non-zero value of the skewness implies an asymmetric distribution with the sign and magnitude a description of this asymmetry. Its numerical estimation is

$$m_3 = \frac{1}{\langle w \rangle^3} \frac{1}{N} \sum_{i=1}^N [h_i - \langle h \rangle]^3$$

4. m_4 is used to calculate the kurtosis which is $(\frac{m_4}{m_2^2})$. The division makes that the kurtosis is a normalized dimensionless value. The kurtosis describes the deviation from a Gaussian distribution (kurtosis value is 3)[13]. Its numerical estimation is

$$m_4 = \frac{1}{\langle w \rangle^4} \frac{1}{N} \sum_{i=1}^N [h_i - \langle h \rangle]^4$$

The use of especially higher order moments has to be done with great care. Just a few (dust) particles on the surface that are easily recognized as extreme heights in the image will alter the determined value of rms and especially the skewness and kurtosis. The small area (less than a percent of the image) of these extremities makes that they are not visible in the histogram itself. With the analysis program Gwyddion these extremities can be eliminated from the calculations.

2nd Order Statistics

In second order statistic the relation between various heights at a specific length scale on the surface is investigated. The basic idea behind this is that although points on the opposite side of an image can strongly vary in height, whereas points that are within each other vicinity can differ in height only by a limited amount. The maximum difference at a large distance is directly related to the rms roughness of a surface. The lateral distance on which the heights can differ by an amount smaller than this maximum difference is called the correlation length ξ . The smaller the value of ξ , the rougher the surface is [13]. Another parameter that determines the surface morphology is called Hurst or roughness exponent α . The Hurst exponent determines how jagged the surface is and introduced by researchers who study the self-affine fractal geometry [13]. It characterizes the irregularity of the surface and its values range is $0 < \alpha < 1$. Large values of α correspond to a smooth hill-valley structure though small values correspond highly irregular surface [14].

There are three basic, related, statistical depictions of this lateral relation between height: the autocorrelation, the height-height difference and the Power Spectral Density function. In our study we made use of the first two only. Because an AFM image is in essence a sequential probing of linescans, the analysis is limited to the fast scan directions, which in our case is the x axis. The results are an average of these fast scan spectra in the slow scan direction.

The 2D autocorrelation AC on a surface with a height profile $h(x,y)$ is defined as:

$$AC(\tau_1, \tau_2) = \iint_{-\infty}^{\infty} h(x, y) h(x + \tau_1, y + \tau_2) dx dy$$

In a numerical implementation over the fast scan direction, x-axis, of a NxN image for the AC for a distance r_m :

$$AC(r_m) = \frac{1}{N(N-m)} \sum_{l=1}^N \sum_{k=1}^{M-m} h_{k+m,l} h_{k,l}$$

The value of $AC(0)$ is the variance or rms^2 value found from first order statistics.

The height-height correlation (HH) in the fast scan direction is defined as:

$$HH(r_m) = \frac{1}{N(N-m)} \sum_{l=1}^N \sum_{k=1}^{M-m} (h_{k+m,l} - h_{k,l})^2$$

The relation between the AC and HH is clear when writing out the above formula. It gives $HH(r_m) = 2w^2 - 2AC(r_m)$. The reason for using the Height-Height correlation is that on a log-log scale a few of the basic parameters can be determined in a graphical manner. This will be illustrated below.

Models for surface roughness

Several models that describe the relation between roughness and lateral length scale have been developed. A frequently used model to characterize the morphology of a thin film is the self-affine model. This model is related to fractal concepts, which states that the morphology looks (on a statistical scale) similar when the length scale is stretched. In other words, the observed morphology is scale invariant. This scale invariance is limited by the finite roughness observed on a surface. With this concept, the Height-Height variation can be described for small and large lateral length scale as:

$$HH(r) = 2w^2 f\left(\frac{r}{\xi}\right)$$

With a scaling function f , which has the properties

$$f(x) = \begin{cases} x^{2\alpha} & \text{for } x \ll 1 \\ 1 & \text{for } x \gg 1 \end{cases}$$

On a log-log scale the three parameters w , ξ and α can graphically be determined, see figure [down].

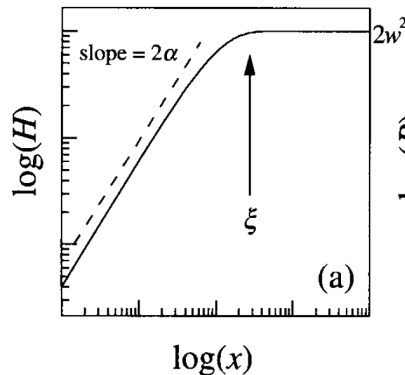


Figure 4: HHCF in a logarithmic scale[13].

For an isotropic self-affine surface, a functional relation for the Height-Height correlation has been proposed [15]:

$$HH(r) = 2w^2 \left(1 - e^{-\left(\frac{|r|}{\xi}\right)^{2\alpha}} \right)$$

With this expression, the AC is easily derived:

$$AC(r) = w^2 e^{-\left(\frac{|r|}{\xi}\right)^{2\alpha}}$$

Adhesion

Adhesion is the tendency of different surfaces to stay in contact [16]. In our point of view it applies in a more specific character. It is the mechanical force that is required for separating two bodies being in contact. This pull off force is measured in our essay between a flat Si tip with a 2 μm diameter that is contact with a CrN surface by using Atomic Force Microscopy. In practice we send the tip to approach the surface. At some point due to Van der Waals forces the tip snaps in to the surface. The tip is pressed on the surface. Then the tip is retracted. At some point it snaps off the surface. Monitoring of the tip from approaching till snaps off gives us the information for adhesion. Below we discuss in more detail the parameters that describe the adhesion measurements.

Surface Forces

Adhesion is a surface property that stems from the interatomic and intermolecular surface forces. These forces are dependent on the physical and chemical properties of the surface materials. The most important forces are: the Van der Waals forces, the capillary forces, chemical forces and electrostatic forces. These chemical and electrostatic forces are negligible compared to the Van der Waals and capillary forces for adhesion measurements.

Van der Waals forces are the summation of three different forces that exerted between atoms or molecules and are all proportional to $1/r^6$ with r being the position between the atoms or molecules. These three different forces are caused by dipole interactions. These interactions are [16][1]:

- The Keesom interaction, which describes the interaction between two permanent dipoles that are rotated to oscillate freely. It is named also orientation interaction.
- The Debye interaction, which describes the interaction between a permanent and an induced dipole. It is named also induction interaction
- The London interaction, which describes the interaction between two induced dipoles that are created by a temporary polarization of the molecules or the atoms. It is named also dispersion interaction.

The Van der Waals forces have a range from ≥ 10 nm to 0.2 nm [16]. The attractive Van der Waals forces is the summation of Keesom, Debye and London interaction forces and thus are proportional to $-1/r^6$. From theory we also know that the van

der Waals force between any two condensed surfaces in vacuum or in air is always attractive.

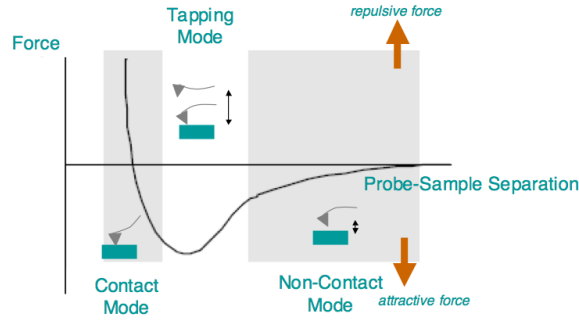


Figure 5: Van der Waal Forces versus distance between tip and sample [image taken from http://asdlb.org/onlineArticles/ecourseware/Bullen/SPMModule_BasicTheoryAFM.pdf].

Capillary forces or meniscus forces induced due to capillary condensation between and around the tip and surface area. In ambient conditions one (or more) layer of water is bound on every solid surface. As a result an attractive force between the tip and the surface is created. The Kelvin equation describes the curvature of the liquid as a function of pressure:

$$RT \ln \frac{P}{P_0} = \gamma V_m \left(\frac{1}{R_1} + \frac{1}{R_2} \right)$$

Where R is the gas constant, T is the temperature, V_m is the molar volume of the liquid, P/P_0 is the relative humidity for water [1][17]. The parenthesis describes the surface curvature of the meniscus.

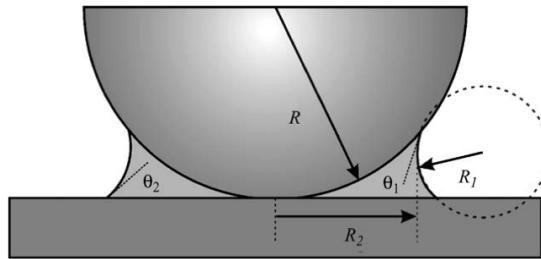


Figure 6: Scheme of a water meniscus between a sphere, which is the tip, and a plate, which is the sample surface [1].

In AFM a water meniscus is formed between tip and sample when the distance between them is in the same scale as the Kelvin radius [12]. The Laplace equation gives the difference in pressure because the pressure inside the meniscus is lower than the pressure outside [17]:

$$\Delta P = \gamma \left(\frac{1}{R_1} + \frac{1}{R_2} \right)$$

The capillary force induced by the pressure difference between the liquid and vapor form of water and could be in the nN range. This force is equal to [1]:

$$F_{cap} = 2\pi R\gamma(\cos\theta_1 + \cos\theta_2)$$

Adhesion measurement with AFM

The cantilever is the key element of the atomic force microscope. In our measurements we take advantage of its mechanical properties in order to characterize our surfaces. These mechanical properties can be simplified to a simple spring-mass system and can be characterized by its spring constant, k , and its resonance frequency ν_0 [20]:

$$k = 2\pi^3 l^3 w \sqrt{\frac{\rho^3}{E}} f_0^3$$

Where l is cantilever's length, w is its width, f_0 is the resonance frequency, E is the Young's modulus of elasticity and ρ is the mass density of the material that is made the cantilever.

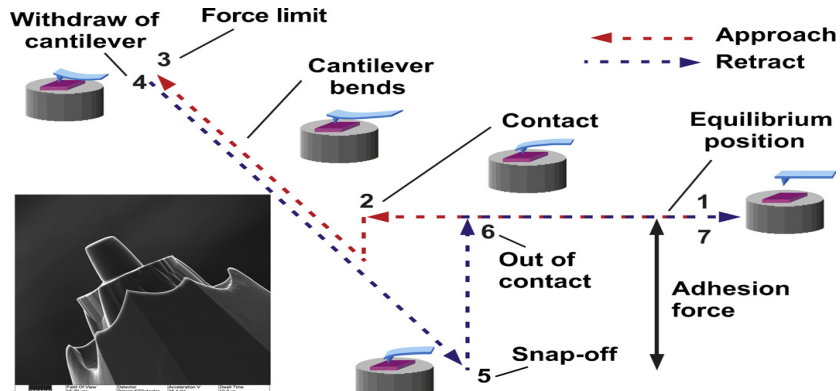


Figure 7: Voltage versus distance measurement. The red color indicates the approaching and the blue color the retracting [29].

In figure 7 is depicted the procedure for the adhesion measurement. In position 1 the cantilever is in no contact with no force to exerted to it i.e. zero deflection. The cantilever and the capillary forces are moving towards the surface. At some point the cantilever due to attractive Van der Waals forces snaps in to the surface at point 2. At this point the gradient of attractive Van der Waals forces exceeds the cantilevers spring constant. The piezo at point 3 moves further the cantilever towards the surface and at point 4 after a maximum approach the piezo starts to retract the cantilever till point 5. At this point the cantilever is still in contact with the surface and due to adhesion force we observe an offset between the snap in and snap off at the contact point. The piezo keeps moving upwards the cantilever till the cantilever force exceeds the adhesion force. The value of voltage between points 5 and 6 is the one that gives us the strength of adhesion force that the cantilever force exceeds [1].

Instrumentation: How to convert Voltage to Force measurement

In order to measure the adhesion force we need to use a method that can provide force measurements in the scale of nN. The advantage of the AFM is that the interaction between tip and sample are monitored and thus with AFM we can perform force spectroscopy. In previous studies [21] the AFM force distance measurement are indicated for adhesion forces determination.

The size of the tip determines the sensitivity of the adhesion measurement. From previous experiments [22] we know that the adhesion force value is proportional to the probe area.

The output of the cantilever's deflection is given as a voltage-distance characteristic. The voltage is proportional to the photodiode current that is induced by the position change of the laser spot, and the position of the height of the piezoelectric translator [1]. In order to retrieve force-distance characteristics from the voltage-distance measurements, we measure the sensitivity. The sensitivity of the cantilever is proportional to the slope of the deflection of the cantilever while the cantilever is in contact with the sample. This is measured from the following formula [12]:

$$\sigma = \frac{\Delta z}{\Delta V}$$

This can be easily measured by measuring the slope of the line between points 4 and 5 in figure 7 and the inversion of it. In addition due to the physical properties of the cantilever we can predict the force from graphs like figure 7.

From Hook's law:

$$F = kx$$

Where F is the force that we are looking for in Newton, k is the spring constant of the cantilever in N/m, x is the distance. From deflection relation we can substitute the distance to the Hook's law and thus we get:

$$F = k\sigma\Delta V$$

In this case ΔV is the blue vertical line between point 5 and 6 in figure 7 that indicates the snap off of the tip from the surface. Thus F gives us the adhesion force in nN.

The use of a Si flat probe, which is hydrophilic, indicates that many small menisci can form between the tip and sample that create more stable capillary necks that occur for more time compare to a sharp tip [22]. Also from previous measurements [22] found that contact force (within boundaries of no deformation) and contact time do not influence the adhesion measurements for flat and rough Si surfaces and we can conclude that holds the same for our study cause similar tips and AFM used. What influenced the adhesion was the velocity of the piezo to which the cantilever was mounted and the relative humidity

In addition, roughness has an influence to adhesion as also mentioned in previous studies [22][23]. From these studies made clear that the adhesion force is inversely

proportional to rms roughness in theory and experiments. Theoretically the relation between the roughness and the asperity radius indicates to decrease the adhesion magnitude as the roughness, and consequently the asperity radius, increases. Geometry of the cantilever also affects the measurements. In the case of a smooth flat tip with diameter in the μm range its clear that the roughness in nm range will affect the adhesion measurements due to difference in penetration of the tip in the asperities of the sample [1]. In contact with a smooth surface sample the adhesion, as an assumption [1], increases due to high particle adhesion in valleys. Rough surfaces have high surface energy of atoms on an asperity surface that may be cause the change of the adhesion. An atom in a plane crystal surface has less 'atomic' surface energy than an atom near an asperity peak or fine fractal surface [24]. Consequently for the contact angle measurements roughness changing affects also the spreading energy (or coefficient) that causes a tendency for not spreading. The spreading coefficient is the summation of the surface tension (or surface energy) of the air, solid and liquid that assembles the system that we study [24]. The hydrophobicity of the sample is increasing with roughness resulting to a decrease of the capillary force as well. The reason is that as the roughness is increasing the capillary condensation that takes place at the nano-structures of the asperities and the flat tip leads to smaller and more in number menisci, which are easier to overcome the tip with less force. In contrast with the smoothest surfaces we get one larger meniscus [1].

Contact Angle

In order to quantify the wettability of a surface we use contact angle measurements. The contact angle is the angle between the tangents of the liquid-fluid interface with the tangent of the solid interface as depicted in figure 8. In our study we used high purity water from a Millipore simplicity IPS system. In one case the liquid has high affinity with the material and therefore can easily spread resulting a low contact angle. In opposite case the material has low affinity with the material resulting a high contact angle. More specifically for contact angles with values higher to 90 degrees we can characterize the surface hydrophobic while for values lower to 90 degrees hydrophilic [25].

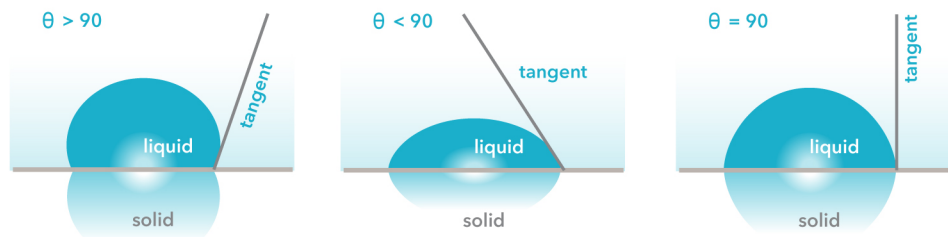


Figure 8: Contact angle of a solid-liquid system in air ambient conditions [image taken by <http://www.attension.com/applications/measurements/contact-angle>].

When the volume of the droplet is increased the contact angle increases as well while the contact line is pinned. The advancing contact angle is reached when the contact line start to move. When on the other hand the volume of the droplet is decreased and the contact angle decreases as well while the contact line remain pinned. The final value is called receding contact angle and is reached when the contact line start to move. The difference between the advancing and the receding contact angles is called the hysteresis range. Roughness has an influence on the contact angle and hysteresis range. Thus is possible to change the wetting properties of a surface simply by changing its morphology. The cosine of the contact angle indicated by the Young relation:

$$\cos\theta_y = \frac{\gamma_{SF} - \gamma_{SL}}{\gamma_{LF}}$$

Where S indicates the solid, F the fluid, L the liquid and γ the surface tension between them[26]. From Young's relation we can determine the influence of roughness on wetting through Wenzel's relation:

$$\cos\theta_w = r\cos\theta_y$$

where r is the roughness of the surface material and θ_w is the apparent angle [25]. The main assumption is that we have a chemically homogeneous surface and that the roughness range is much smaller than the droplet size.

Resistivity

In order to understand how the change in surface morphology affects the resistivity of our surface samples we have performed four probe resistivity measurements. We applied the Van de Pauw method [26], which is briefly addressed in the experimental section. Previous studies on metals [27] have revealed that there is a firm relation between surface conductivity and surface roughness:

$$\sigma = \frac{\sigma_0}{1 + sw}$$

Where σ is the conductivity (σ_0 its initial value), s a normalization material factor and w the rms roughness. Consequently through the resistivity and conductance relation [28]:

$$\rho = \frac{1}{\sigma}$$

It is clear that resistivity should be proportional to roughness. The surface conductivity, σ , depends on density of electrons and holes (n,p) as well as their mobilities (μ_e, μ_h):

$$\sigma = e(n\mu_e + p\mu_h)$$

Where e is the electron charge, n the electrons density, p the holes density and μ their mobility in perspective. An increase of the surface roughness leads to an enhanced scattering and therefore the mobilities will decrease.

Experimental Set-Up and Methods

Sample Preparation

In order to sputter our samples we place them into a vacuum chamber. Before the placing we cleaned them. Each of the CrN samples has a dimension of 10x10 mm and is 0.75 mm thick. In order to place them on the sample holder for ion bombardment, we glued them on Si samples with a 30x5 mm surface. Before gluing the Si and CrN samples were cleaned with acetone for 15 minutes in an ultrasonic bath. After the bath the samples were boiled in isopropanol at 90^o C and dried with N₂. Then we glued the two samples using Varian Torr Seal epoxy. This is solvent-free epoxy and can be used at pressures of 10⁻⁹ mbar. The next step is the placing of the sample in the vacuum chamber for ion bombardment.

System Description

In figure 9 the system used for ion bombardment is shown. More specifically picture shows:

- The vacuum chamber that includes the sample holder.
- The goniometer that allows the sample holder to be rotated to a precise angular position in the azimuthal axis with respect to the ion source.
- The ions source that is a Tectra Gen Plasma Source.
- The magnetron and the extraction controller of the ion source, Tectra Gen Plasma Source.
- The turbo pump under the vacuum chamber that creates the vacuum.
- The pump control.
- The Argon supplier that introduce the inert gas into the ion source chamber.
- The pressure gauge that is a Varian Multi-Gauge Controller.

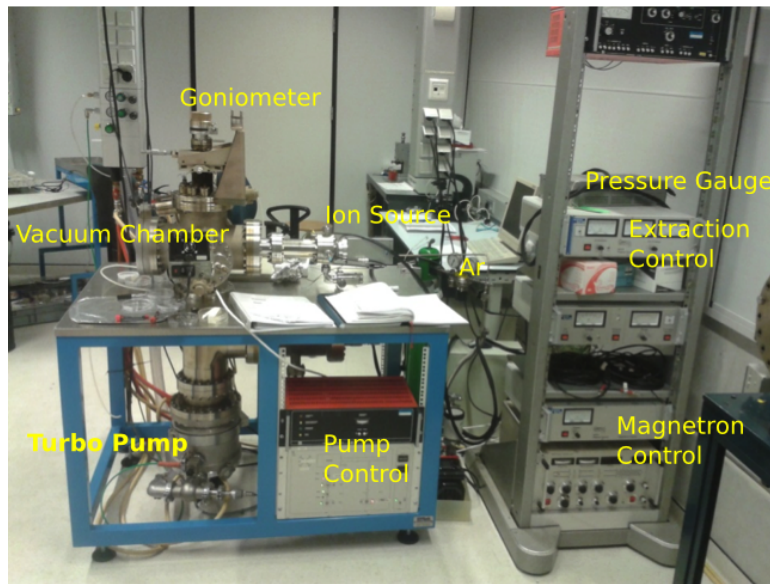


Figure 9: Sputtering and pumping system.

Ion Bombardment

In this essay we try to change the morphology of the CrN surface samples using ion bombardment i.e. ion beam sputtering. In order to sputter our samples we used a tectra plasma ion source (figure 10) attached to the vacuum chamber. The open end of the plasma grid is closed with a grid of holes made from molybdenum. The distance between the sample holder and the grid is 4 cm. The sample is positioned in the sample holder that has the ability to change the polar angle of incidence of the ion beam. The initial angle corresponding to the plasma grid is 180° so the sample initially is protected from the plasma ions. After the preparation of the plasma the goniometer is set at 0° and we sputter our sample at normal incidence.

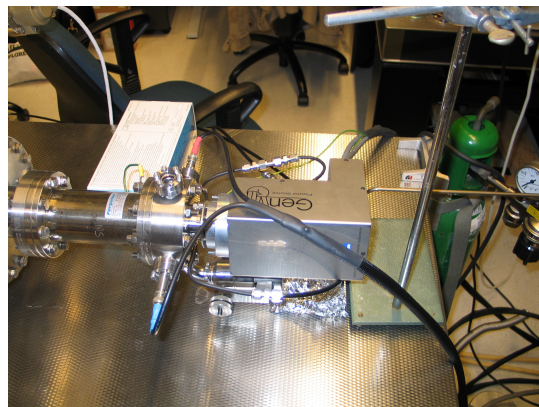


Figure 10: Gen tectra plasma ion source installed at the HV chamber.

The background pressure of the vacuum system is in the 10^{-8} mbar range. After Argon gas is introduced in the ion source chamber the pressure increases to 10^{-5} mbar. Then we switch on the magnetron supply of the tectra plasma source. An initial value for the magnetron current is set at 25 mA. After 10 to 20 minutes, depended on the plasma color, which should be purple, we are ready to sputter. At this point we increase the magnetron supply current to 35 mA and the extraction voltage to -0.4 V. An ion energy of 1.5 kV is used.

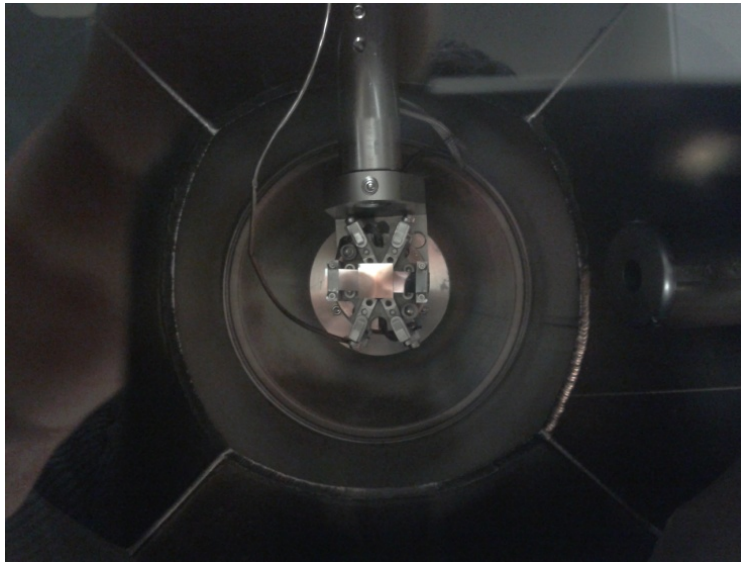


Figure 11: CrN sample placed on the sample holder in 180° angle position. Behind it is the grid of the ion source.

We sputtered CrN samples for 5, 10, 20, 30, 45 and 60 minutes at the same sputter conditions. The measured values of fluence and flux for the ion source with Ar^+ are 7.31×10^{18} ions/cm² and 326 $\mu\text{A}/\text{cm}^2$ respectively measured with the Faraday cup method. These numbers are used as a reference as the continuous use of the ion source causes cracks at the metals that consist the grid that result in a decrease of the sputtering efficiency.

Atomic Force Microscopy

In order to observe the changes upon in sputtering, in terms of roughness and adhesion, both topography and force-distance measurements are performed. For topography and force-distance measurements an AFM 5100 Agilent is used [figure 12] at ambient conditions, 21 °C and 40% relative humidity.



Figure 12: Agilent 5100 Atomic Force Microscope.

Topography imaging

The surfaces were imaged with AFM operated in intermittent contact mode. The monolithic silicon cantilevers (Tap190DLC) have a diamond-like carbon coating tip, 15nm thick. These are long hydrophobic tips with high durability. Their upper side is coated with an Aluminium layer in order to gain higher reflectivity (figure 13), 30 nm thick. These tips are sufficiently sharp to image the smallest features of interest in a range of 5 nm.

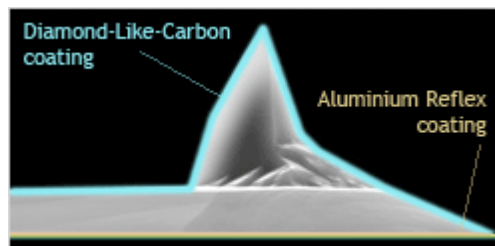


Figure 13: Coating of a Tap190DCL tip. Image from the manufacturer's website.

The tips dimensions are: 17 μm high, 15 μm set back and a radius smaller than 15 nm as depicted in figure 14.

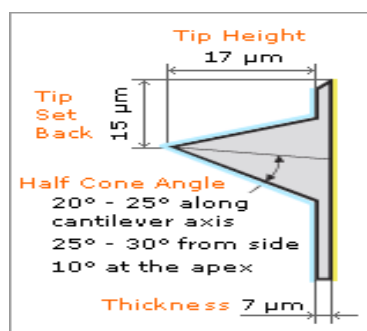


Figure 14: Dimensions of Tap190DLC tip. Image taken from manufacturer's website.

The cantilever dimensions are: 225 μm length, 38 μm width and 7 μm thickness. The spring constant is 48 N/m. The resonant frequency given by the manufacturer is 190 kHz but in the lab measured 165 ± 3 kHz. In addition after every scan a sensitivity measurement performed for comparison.

For every scan we get an image that depicts $20 \times 20 \mu\text{m}$ with 4096×4096 data points (pixels). The scan speed was constantly set to 1 line per second with x axis to be the fast scan dimension and y axis the slow one. The deflection was always under 0.8 V and over 0.6 V. The friction was always under 2.5 V and the Amplitude between 0.3 and 0.5 V.

From a measured topography to statistical quantities

In order to gain the statistical quantities from the raw AFM data we made use of Gwyddion v2.30. Gwyddion is a freeware program that is commonly used for the analysis and manipulation of SPM images. The raw images are strongly hampered by a slope and the bow of the scanner. Also the individual line scans do not smoothly align (note that this the reason for evaluating second order statistics only in the fast scan direction). The correction performed to the raw images were in the following order:

1. Match line correction, which performs a line correction in the fast scan direction.
2. Plane level correction, which removes a plane with the condition that the average is zero.
3. Mask outliers, this masks all image points that exceed a specific height. It is used to avoid influence of bumps and dirt on the numbers of the first order statistics.
4. Background removal, a 3rd order polynomial correction is used with the condition that the average height is zero. This compensates for the bow of the scanner.

Force-Distance Measurements

In order to measure the adhesion we used force-distance spectroscopy in AFM. In force distance measurements we monitor the movement of the tip in the z axis (figure 16 from [29]). In addition we did measurements for two time values, 2 and 20 seconds that mainly affect the velocity of the piezo. The choice was made to measure at two different piezo velocities 0.3 and 0.03 $\mu\text{m}/\text{sec}$. The values chosen gave a good difference in adhesion for rough and smooth silicon [22]. The force that exerts the piezo to the cantilever is in the μN range and is constant for all the measurements,

For this kind of measurement we used flat silicon tips, named PL2-NCLR-10 that originates from PLateau tip -Non-Contact /tapping mode - Long cantilever - Reflex coating. The tips are made by single crystalline n^+ doped silicon in order to dissipate

static charge. The plateau diameter is typically $1.8 \pm 0.5 \mu\text{m}$ and on detector side of the cantilever an Aluminium coating was deposited. These tips are, according to the manufacturer, chemically inert.

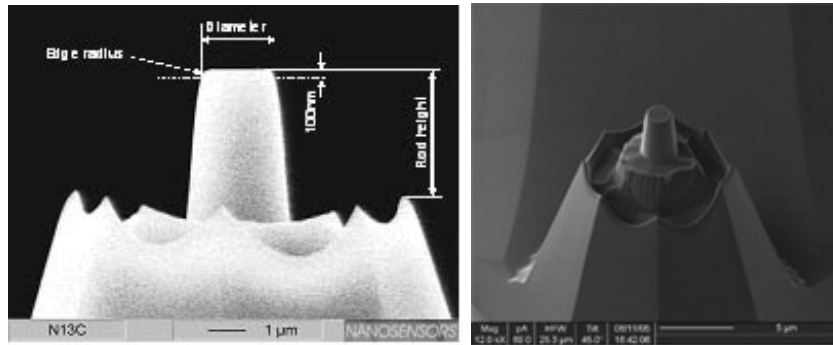


Figure 15: PL2-NCLR-10 flat silicon tip images. Image taken from manufacturer’s website.

The tip dimensions are: $1.8 \pm 0.5 \mu\text{m}$ plateau diameter, $>2 \mu\text{m}$ plateau rod height, $0.3 \pm 0.1 \mu\text{m}$ plateau edge radius, $12.5 \pm 2.5 \mu\text{m}$ tip overall height. For this kind of silicon tips a silicon oxide of a few layers is usually created on the outer side of the tip surface in ambient conditions [1] Thus the tip can be characterized as hydrophilic.

The cantilever dimensions are: $7 \pm 1 \mu\text{m}$ thickness, $38 \pm 8 \mu\text{m}$ mean width, $225 \pm 15 \mu\text{m}$ length, $35 \pm 10 \text{ N/m}$ force constant, $190 \pm 46 \text{ kHz}$ resonance frequency.

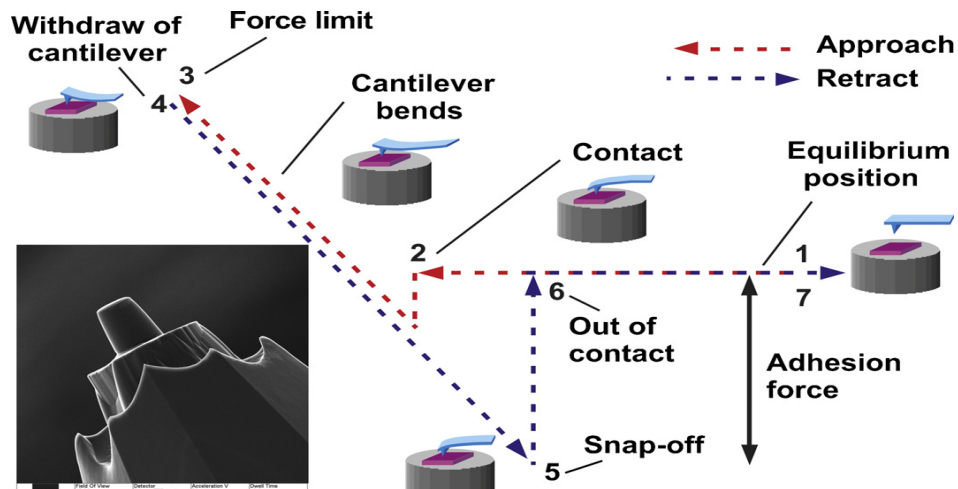


Figure 16: The adhesion measurement as depicted as a function of position (x axis) and voltage (y axis) [29].

In figure 16 the sequence of a force-distance measurement is depicted. The cantilever approaches the surface (1) and at some point due to van der Waals forces the tip snaps to the surface (2). Then the AFM piezo exerts more force on the cantilever and the cantilever bends (3). At some max force point the piezo is retracted the cantilever starts to withdraw (4). Then at some point the tip snaps-off the surface (5) and the cantilever is out of contact (6)



Figure 17: Force distance spectroscopy measurement on a CrN sample. The x axis measures the tip position and the y axis the voltage value that the photodetector creates.

In figure 17 a measurement image, taken with the Pico-View software, shows one force distance measurement. In the y axis the voltage is measured and in the x axis the tip's position. The difference between snap in and snap off is 26 nm. This image depicts the force distance measurement for 20 seconds. The parallel alignment of the flat tip to the sample is crucial for a successful adhesion experiment.

For every sample we first search for the highest value of adhesion by fitting the sample's position with respect to the cantilever. This ensures a parallel geometry between tip and sample. Then we perform 10 force-distance measurements, which provide 10 adhesion values. The average of these 10 measurements and their standard deviation are used. At this point is crucial to mention that in our measurements the distance between points (1) and (4) in figure 16 was for all measurements 0.6 μm . In addition adhesion measured with a flat-sphere 1 μm radius silicon probe.

Contact Angle Measurements

In order to determine our surface samples as hydrophobic or hydrophilic we performed contact angle measurements. The contact angle of the surfaces measured with an OCA15+ goniometer. OCA15+ creates microliter droplets with a computer-controlled syringe. The set-up is depicted in figure [down]. The droplet volume is 1 μl . The volume reproducibility in the μl range is within 5%. A camera is used to characterize the in terms of contact angle with 0.5° accuracy. The static contact angle is measured after droplet deposition. Both advancing and receding contact angles are measured by increasing and decreasing the droplet volume with 1 μl .

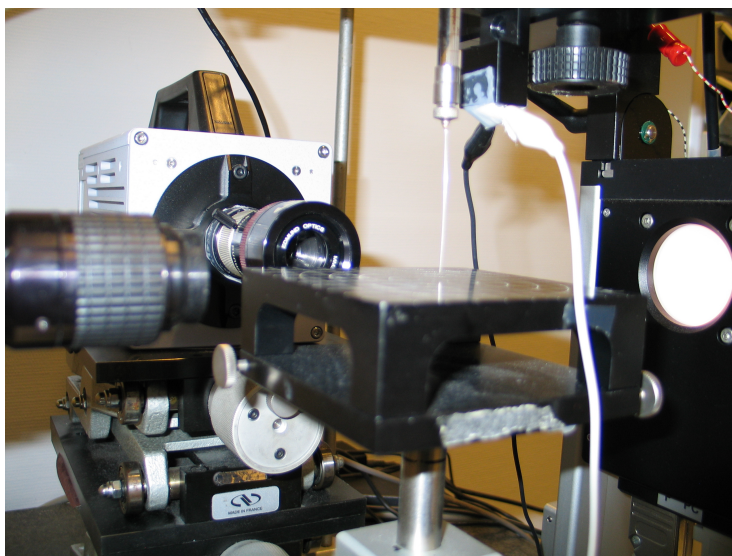


Figure 18: OCA15+ goniometer. On the left is depicted the camera, in the right the light and in the middle the syringe that is connected with the computer.

In figure 19 the measurement procedure is depicted. In the first image the syringe deposits a 1 μl droplet. At the second picture the droplet is on the surface in balance without the syringe touching it and then we measure with the goniometer the contact angle. At the third picture we place the syringe back to the droplet and we add 1 μl more. Then we measure the advancing angle at its maximum volume in picture four. After this we introduce the syringe again and remove 1 μl of water. Since the point between the droplet, the surface and the air start to move we measure the receding angle till the droplet has the shape of photo six. At picture seven we observe the droplet after the syringe moves away. The difference between advancing and receding angle provides direct information on the influence of the contact line.

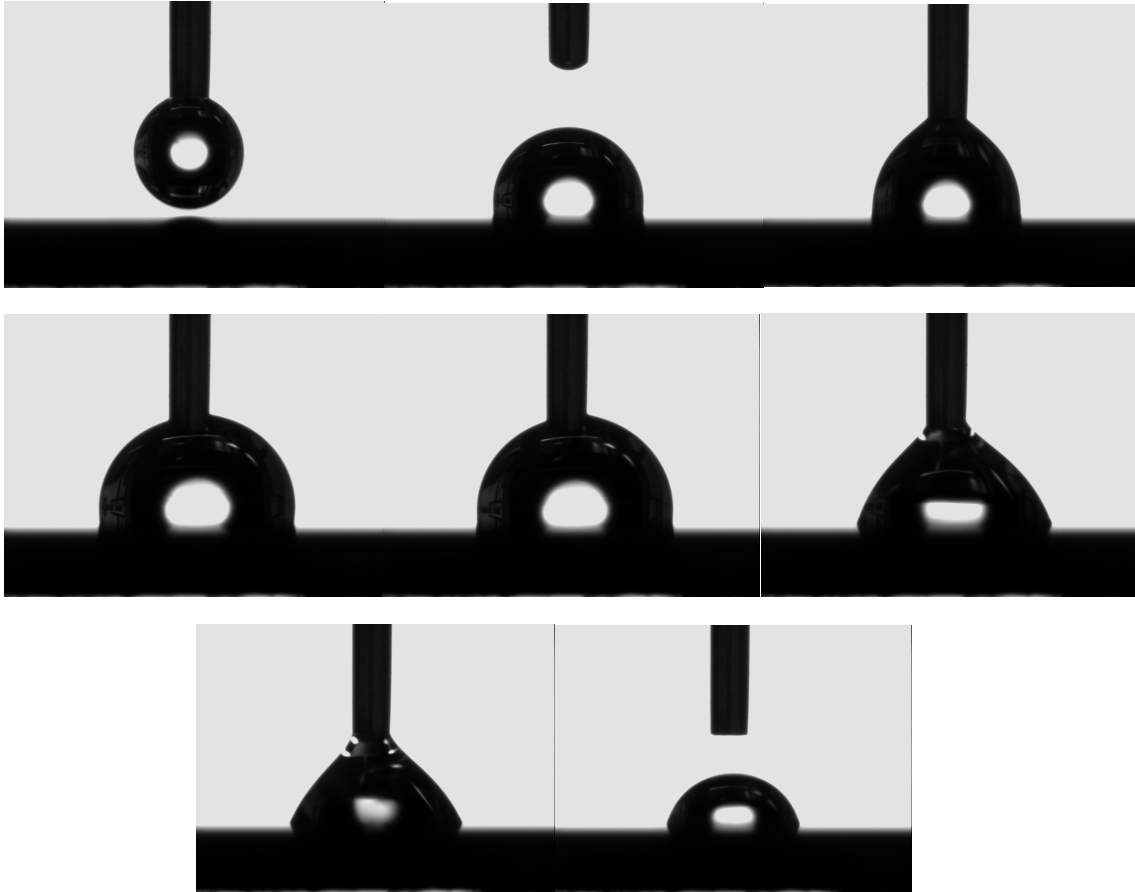


Figure 19: The contact angle measurement (2nd picture). The advancing angle measurement (3rd and 4th picture). The receding angle measurement (5th and 6th picture).

Four Probe Resistance Measurements

In order to measure how the change in topography affects the surface resistance we performed four point probe resistance measurements. This method is known as Van der Pauw method [26]. With this method we press four probes on the sample surface. Each probe can be programmed to perform different functions in terms of current sweep, voltage bias or common. In Figure 20 is depicted the placing and the function of the four probes. The four probes were placed in a rectangular formation. The two down probes were the current sweep and the common. The other two on the upper side were measuring the voltage difference. The voltage difference as a function of the current applied is shown in figure 21.

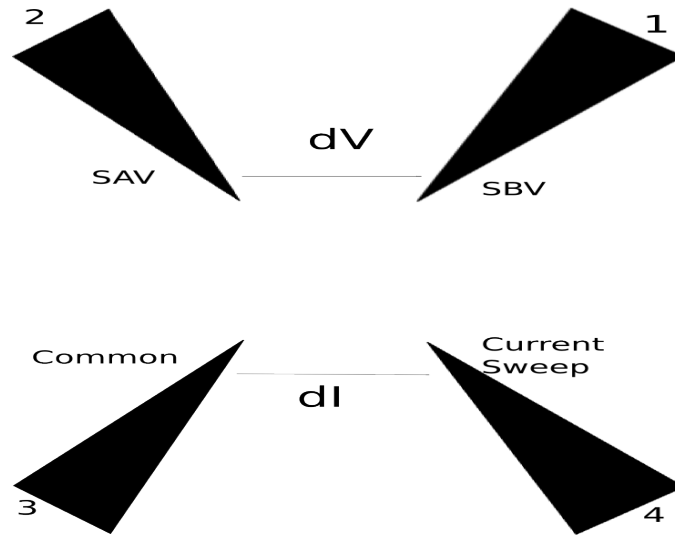


Figure 20: Four probe resistance measurements for CrN surface samples.

The software that we used is KITE and the hardware is a Hewlett Packard 4284A precision LCR meter and allows us to choose which functions should be used for every probe in order to measure the electric properties for every device in terms of current sweep, voltage bias or common. Based on that and also to the fact that we can arrange the values of the current and voltage that needed to apply it is possible to collect information about the electric properties of each sample. In these measurements the current swept from -1 A to 1 A with a step of 0.02 A.

From these measurements we get a linear response of the voltage difference as a function of the current as depicted in figure 21. In figure the current is the x axis entitled SAI. With blue color the voltage is shown entitled DV. For the same graph with red color the resistance is depicted entitled R. From the slope of the blue line the resistance for each sample is evaluated. The reason for not using the high peak value of the red line as the resistance value is due to the non-continuity for some samples. On the other hand for every sample we get a linear response of the voltage as a function of the current.

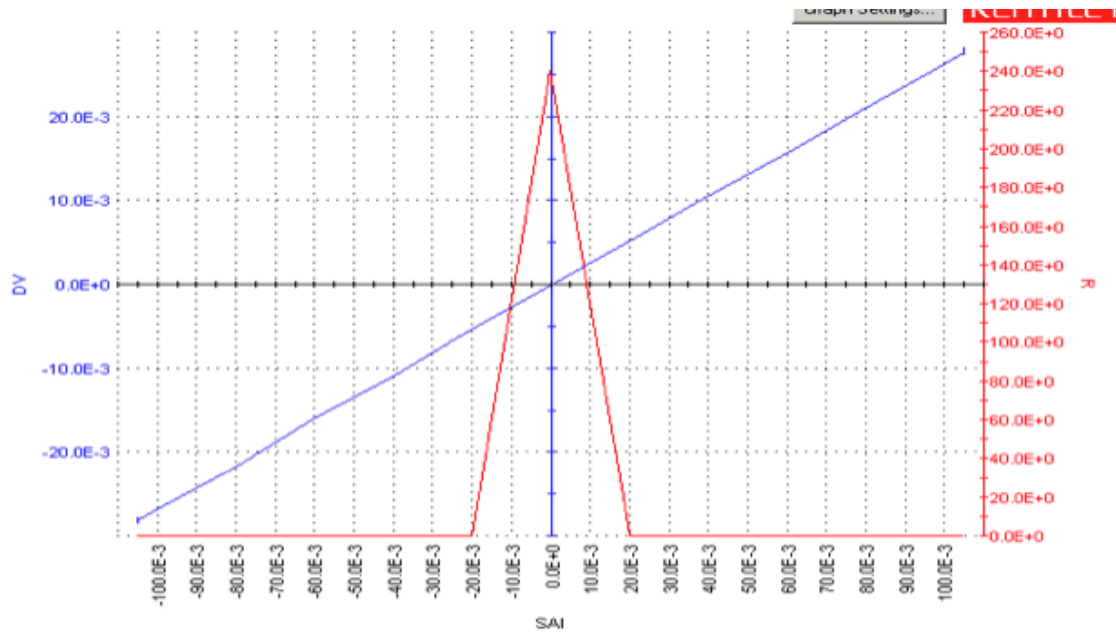


Figure 21: Four probe measurement for the flattened sample. The current is on the x axis entitled SAI. The voltage difference depicted with blue color entitled DV. The resistance entitled R is depicted with red color.

At this point we should mention that it was not possible to measure the exact distance of the probes position with respect to each other but we made sure with a camera that the relative position does not change for all the measurements. In addition it was not possible to determine the pressure that each probe exerted on the sample. A variation in pressure can introduce differences between measurements.

Results and Discussion

Morphology

In order to change the morphology of the CrN samples we used ion sputtering with Ar^+ . Each sample was sputtered for different time. In this study we describe each sample by its time of sputtering. In order to identify the unsputtered initial sample we refer to that as zero minute sample. In addition we performed the same measurements for a flat CrN sample that is less rough comparing to the unsputtered one due to a polishing procedure. We refer to this sample in the time-scale description as polish or flattened or -5 minutes sample.

With tapping mode AFM the topography of CrN samples was measured. Images with a $20 \times 20 \mu\text{m}$ surface with a 4096×4096 pixel resolution were made.

AFM Images

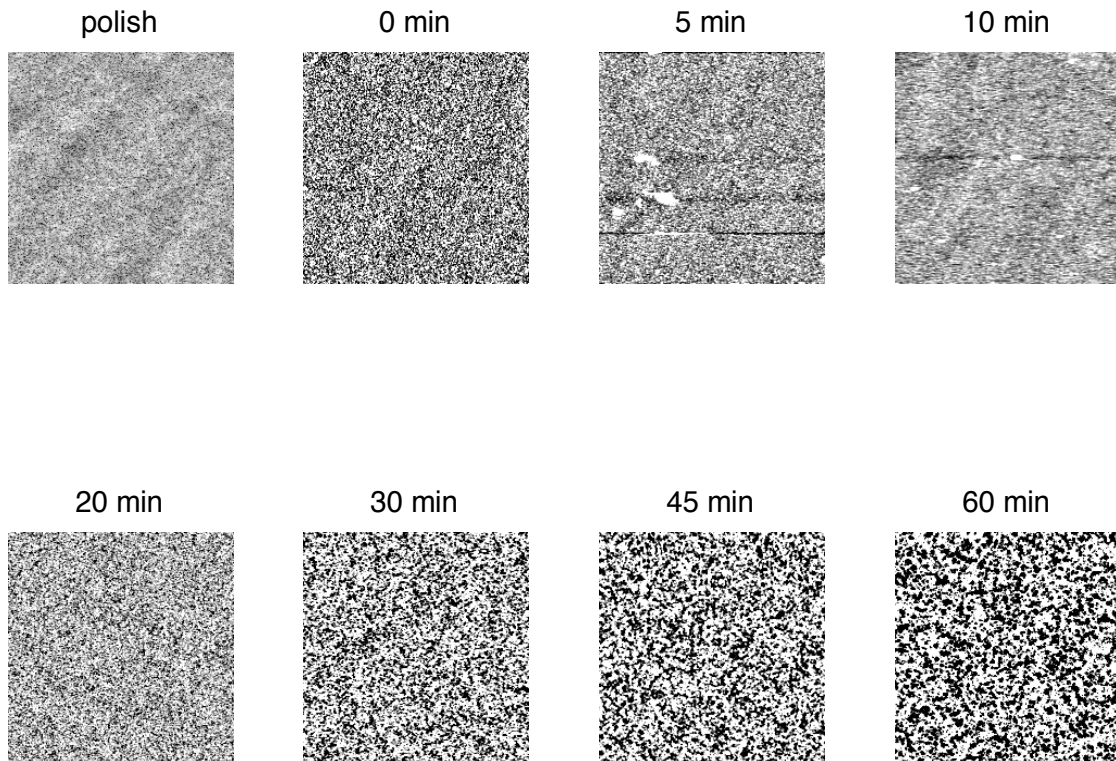


Figure 22: Topography images taken by tapping mode AFM method. Each picture depicts a $20 \times 20 \mu\text{m}$ surface with 4096×4096 pixels resolution for different sputtering time.

In figure 22 the topography images that measured with AFM tapping mode are depicted. These images depict a $20 \times 20 \mu\text{m}$ surface with 4096 pixel resolution.

Normally for topography determination we need more than one the images from different sites of the same surface in order to conclude the reproducibility of the results. This kind of measurements done with different AFM before and the results showed a similar rms roughness for every sample. These images depicted a $5 \times 5 \mu\text{m}$ surface with 512×512 pixel resolution. In addition the HSCF graph from these images made clear the need for more data points in each axis in order to have enough data for the determination of the statistical parameters. Thus we measured a 20×20 surface with high-resolution 4096×4096 .

These images do not indicate the development of a characteristic length scale i.e. no ripple formation is observed. For a more quantitative interpretation the statistical quantities as the surface roughness have to be determined. For the 5 and 10 minutes samples we observe some defects that are probably caused by dirt on the sample's surface. In order to study further the statistical parameters that describe our surfaces we made use of the 1st and 2nd order statistics.

1st Order Statistics

The analysis of the 1st order statistics is based on the histogram that made from the height one dimensional distribution function $p(h)$. The height distribution function provides the probability of a surface height between h and $h+dh$.

In every graph we depict the polished or flattened sample as -5 minute, which is not realistic but is convenient in order to depict it as a function of sputtering time. On the other hand we name the unsputtered or start sample as 0 minutes since it get no sputtering and we use it as a reference sample.

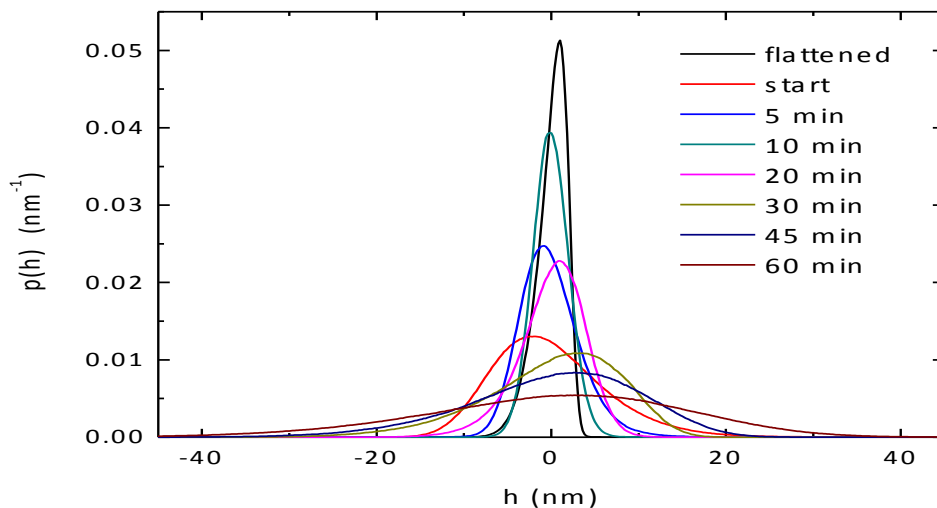


Figure 23: Height distribution function $p(h)$ for different rough surface samples due to different time of sputtering.

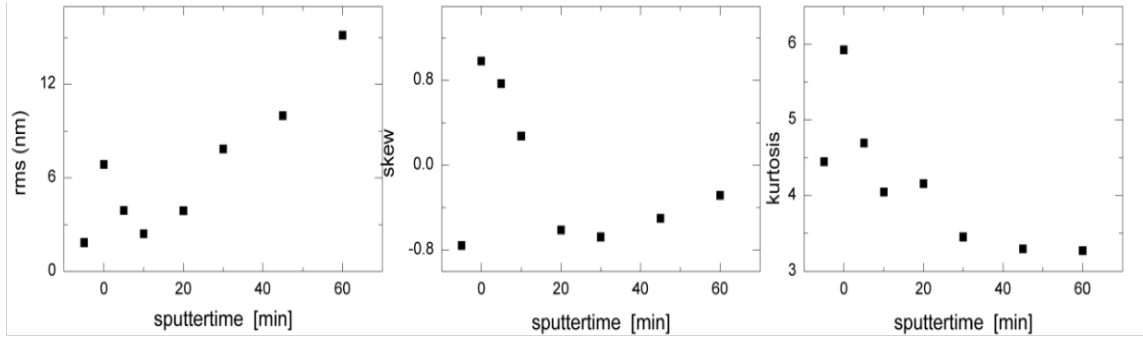


Figure 24: RMS roughness, skewness and kurtosis versus sputtering time.

In figure 23 the height distribution function is depicted corresponding a surface height histogram. The height distribution is a Bi-Gaussian height distribution.

In figure 24 rms roughness, skewness and kurtosis depicted as a function of the sputtering time. For the rms roughness is obvious that the roughness is decreasing for the first 10 minutes of sputtering. This results to a smoothing of the surface. For 20 minutes and further the roughness is increasing linearly. For the flattened sample the roughness is less than the 10 minutes roughness value, which indicates that is the smoothest sample we have.

Skewness is decreasing for the first 20 minutes abruptly and then keep decreasing but more smoothly till the 30 minutes. For 45 and 60 minutes skewness increases smoothly. The crossing of skewness through zero marks a shift in asymmetry [13].

For the flattened sample skewness has the nearest value to zero in the graph.

Kurtosis has a decreasing trend as the sputtertime increases which looks almost exponential. The fact that we get no 3 value for the kurtosis indicates that we have no Gaussian distribution. For the flattened sample kurtosis has a value a bit lower to this of the 5 minutes sample.

The fitting of a Bi-Gaussian distribution gives us statistical quantities for each surface such as: x_c which is the mean height value h corresponding to each distribution, height which is the highest value of the height distribution function $p(h)$ for each sample, w which is the width of the Bi-Gaussian distribution regarding the low (left) half and the high (right) half of the distribution curve. These values are depicted in figure 25.

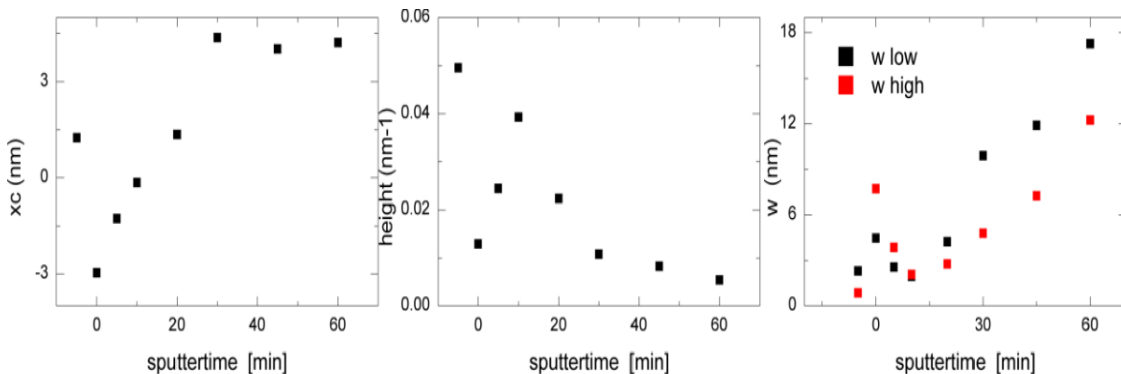


Figure 25: Statistical values acquired after the fitting of a Bi-Gaussian distribution to the height distribution.

From figure 25 we obtain information regarding the height distribution. From the values of x_c is evident that the height distribution function is Bi-Gaussian due to non-zero values of the average height. The value increases for the first 30 minutes and then decreases smoothly for 45 and increases again for 60 minutes. For the flattened sample the height is similar to the 20 minutes sample height with a value over zero.

The height distribution value is increasing for the first 10 minutes and decreases after till the 60 minutes that has the lowest value. For the flattened sample we observe the highest value.

The weight of the Bi-Gaussian has higher values for the high part for the 0 and 5 minutes. For the 10 minutes sample the high and low weight are almost equal i.e. a symmetric distribution. For 20 minutes till 60 minutes the low part has higher values indicating a shifting of the asymmetry. For the flattened sample we observe that the low width has higher value from the high width. For more detailed analysis we performed a 2nd order statistical study.

2nd Order Statistics

The height distribution function, which is 1st order statistics, used for the description of statistical properties of the surface at specific positions. In order to gain further information for the statistical parameters of the surface we use 2nd order statistics that use the correlation of statistical variables from different areas of the same surface [13]. In an attempt to compare our data with these from theoretical models we calculated the height height correlation function for all the surface samples.

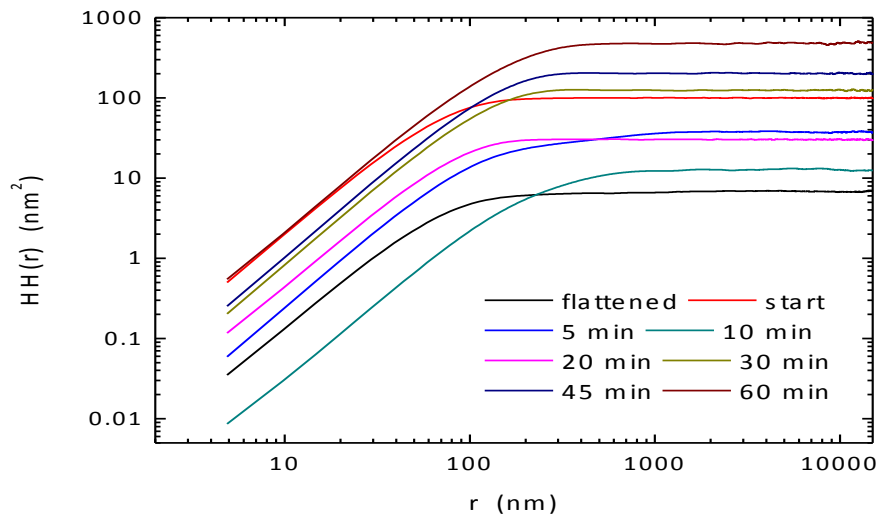


Figure 26: Height-Height Correlation Function for different samples regarding different sputter time.

In figure 26 is depicted the height-height correlation function (HHCF) for different surfaces with different sputtering time. In addition from this graph we conclude that also a $10 \times 10 \mu\text{m}$ image is enough big in order to have enough statistics. From the theory [13] we concluded that the HHCF graphs of our samples have similarities with the HHCF of the self-affine rough surfaces as we see from theory[13]. Though the self-affine doesn't give the best description for our graphs is indeed the most appropriate. From these graphs we are able to determine α , ξ and w . From the graph we observe that on the left part of the graph before the saturation all the lines are parallel except for the flattened sample indicating similar α values. The graph shift is not happening at the same r for all the samples indicating a sifting for the ξ values. The ξ determined as the common spot of the two lines. The oscillations at the right side of the graph are the result of poor statistics at this part of the curve. In addition we calculated the Auto Correlation Function (ACF) for further analysis in order to compare the values for α , ξ , and w . In figure [down] the ACF for every sample is depicted. From the theory we can determine the statistical parameters by fit the graphs. In this figure only normalized ACF curves are shown. Thus from these graphs we determined the rms roughness, the correlation length ξ and the Hurst exponent α . The ACF graphs are depicted in figure 27 for all the surface samples.

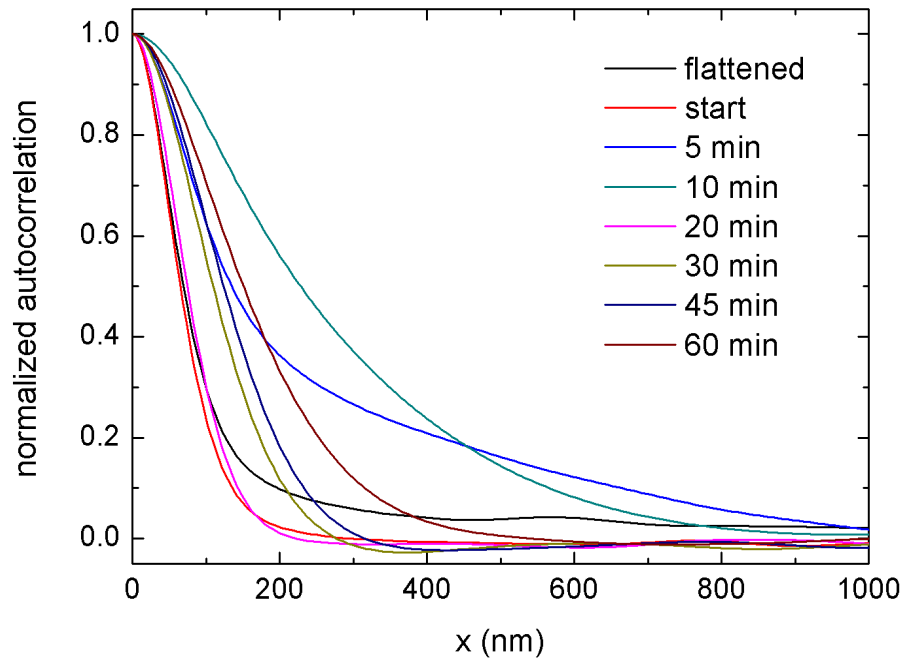


Figure 27: Auto Correlation Function for different time sputtered samples.

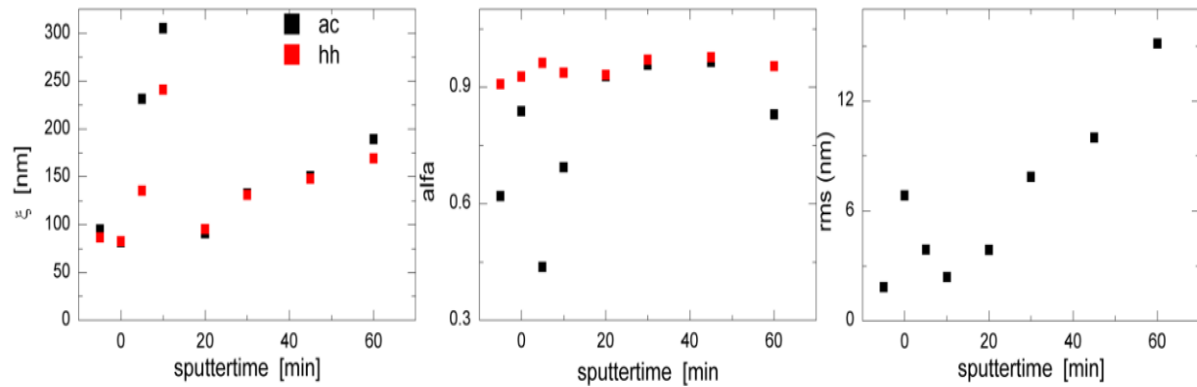


Figure 28: Correlation length, Hurst exponent and RMS roughness values generated by the HHCF and the ACF graphs.

In figure 28 we see the values of ξ , α and rms roughness versus the sputter time. The ξ and α values calculated using the HHCF and the ACF. The ξ is increasing for the first 10 minutes and then decreases at 20 minutes. Then from 20 till 60 minutes we observe an increasing to its value for both the HHCF and ACF.

The α graph presents a similarity in the values with the unspattered sample to have the lowest value and the 45 minutes sample the highest for the HHCF. The same doesn't hold for the ACF in which the α values have very big spread. From the theory is known that the lowest the value of α the roughest or more jagged the surface is since α is describing the sharpness of the wiggles [14]. Based on this and also to the rms roughness values we conclude that the best representation that describe our samples is the HHCF.

The rms roughness values are similar to these that we obtained from the AFM images indicating the proximity of the HHCF. The main problem is, according to the HHCF graphs, that at small scale and at large scale the figures depict a self affine profile but in the medium scale deviations occur. On the other hand for the ACF we observe small oscillations for big scale that indicate ripple formation with small periodicity [13]. This didn't observed from the AFM images though.

AFM Force-Distance Measurements

After the roughness measurements we performed force-distance measurements in order to study how the adhesion force is affected by the morphology changing.

In figure 29 is depicted the adhesion of each sample versus the sputtering time for 2 and 20 seconds contact time. Each point that is shown describes the average value of 10 different adhesion values with the error-bar to describe the standard deviation for each group of measurements. The reason of this high error bar regards the morphology of the sample and the area of the cantilever. In general our sample surfaces are rough and the cantilever is flat. Thus the misalignment of the cantilever flat area surface at the rough sample surface causes a divergence in the adhesion

values. When the tip is in contact with the surface the piezo keep exerts pressure to the cantilever. This causes a slide of the tip on the surface that affects the measurement [1]. Also the meniscus forces that created from capillary condensation between rough surfaces after the contact of the cantilever at the surface is a possible explanation [1]. In addition a small change of the relative humidity influences the capillary forces due to presence of condensed water in the interface between surface and tip. Another factor might be the plastic deformation of the sample in the contact regime due to higher area of the tip that 'hits' the sample, which results to a spatial surface deformation. From figure 29 we observe an increase of adhesion for the more flat samples (5 and 10 minutes) and a decrease for the more rough samples (0, 30, 45 and 60 minutes), which agrees with the theoretical relation between adhesion and roughness [1].

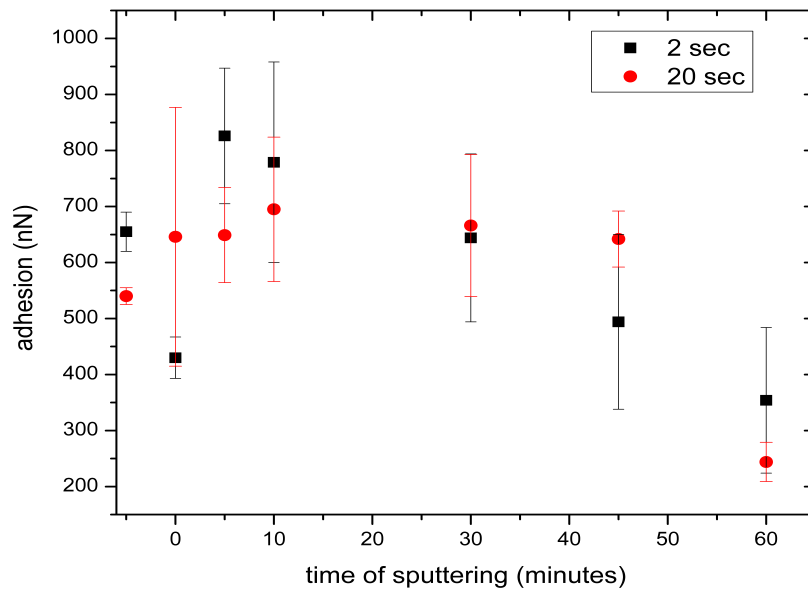


Figure 29: Adhesion force as a function of sputtering time for two different contact time-lengths.

In figure 30 is shown the adhesion versus the rms roughness. We notice again the same influence of the rms roughness on adhesion. The trend of the adhesion according to the graph is inversely proportional to the rms roughness, which agrees with the theory [1]. We conclude an inversely relation between the adhesion force and the rms roughness.

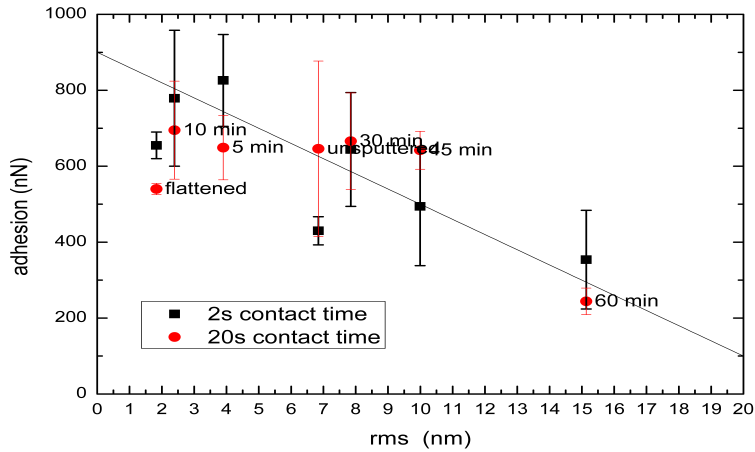


Figure 30: Adhesion force versus rms roughness for two different contact time-lengths.

At this point we are able to determine the adhesion forces between a flat hydrophilic Si tip and a rough surface. It is essential to know if our surfaces are hydrophilic or hydrophobic in order to understand further the relation between tip and surface and how this affect their separation.

Contact Angle Measurements

In order to study the hydrophilicity or hydrophobicity of our samples we performed contact angle measurements using the sessile droplet method. From this experiments we measured the contact angle, which characterizes the surface. In addition advancing and receding measurements were made. Figure 31 shows the contact, advancing and receding angle measurements as a function of sputtering time. Each point depicts a mean value of several measurements on every sample and their standard deviation depicts the error-bar.

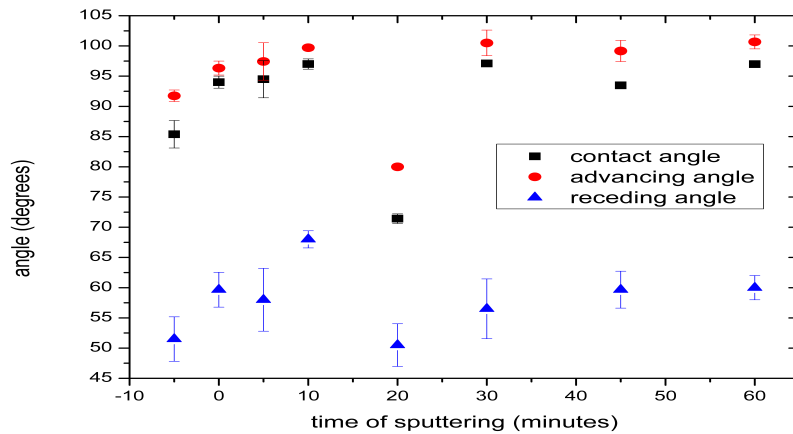


Figure 31: Contact, advancing and receding angle measurements for different surface samples regarding sputtering time.

According to the literature for water contact angles higher than 90 degrees we have hydrophobic surfaces [25] while for water contact angles lower than 90 degrees we have hydrophilic [25]. From the graph we observe the hydrophobicity for almost every sample except the 20 minutes sample. The same holds for the flattened one. Thus from the contact angle we observe hydrophobicity for the rougher samples and hydrophobicity for the smoother samples. Unfortunately the 20 minutes sample shifts the samples surface from hydrophobic to hydrophilic. In figure 32 we depict the hysteresis for each sample, which is the difference of the advancing and the receding angle [26].

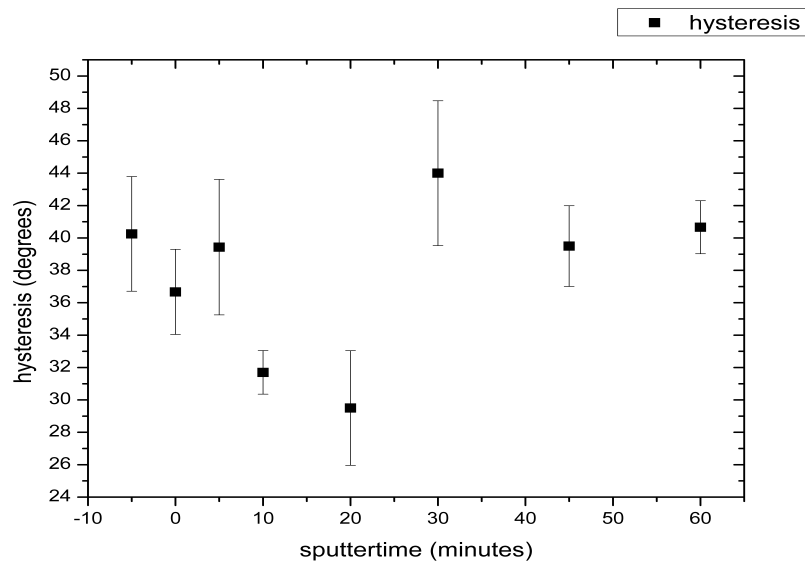


Figure 32: Hysteresis as a function of sputtering time for different surface profiles.

We observe a small increasing of the hysteresis from 0 to 5 minutes and then a decreasing from 10 to 20 minutes. The hysteresis increases and has its highest value for the 30 minutes sample, lowers at 45 minutes and increases for the 60 minutes sample. The big error-bar in the 30 minutes sample indicates a heterogeneous surface [25][26]. In some occasions air bubbles may be trapped in the roughness grooves under the liquid and this affects the contact angle measurement [26]. Also the dirt on the surface may affect the results. Another possibility is that the ion beam might have high divergence on the surface and that might cause the shift in hysteresis as well. As a remark in all the measurements the droplets kept their spherical shape and this indicates that the surface is isotropic.

Four Probe Resistance Measurements

In order to understand how the sputtering affects the morphology of the surfaces in terms of resistance we performed four probe measurements.

In figure 33 the four-probe resistance measurements are shown. Each point depicts one measurement for every sample. From the graph we observe that the resistance is almost constant for the first 10 minutes of sputtering. For the 20 minutes the resistance is increasing constantly till the 60 minutes sample. For the flattened sample the resistance is comparable to the 30 minutes sample. From the graph we conclude that the resistance is increasing as a function of sputtering time.

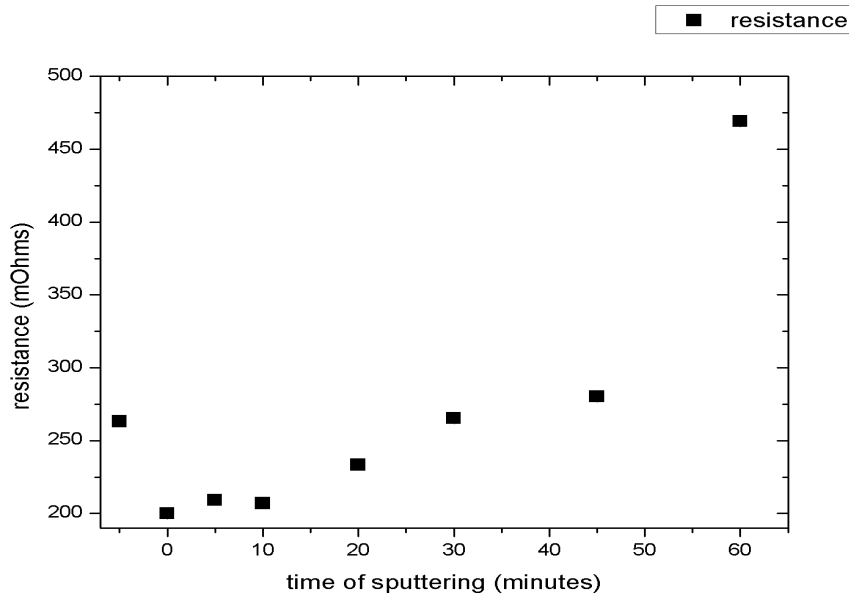


Figure 33: Resistance measurements for different samples regarding sputtering time.

It is crucial though to mention that the difference in the contact load of the probe affects the measurement. There is no way of measuring this and thus the pressure adjustment is empirical. From previous studies in nitride metals also observed the proportionality of the surface resistance with the roughness [30].

Conclusions and Future Perspectives

The surface properties of CrN sample upon ion sputtering were studied with Atomic Force Microscopy, contact angle and four probe resistivity experiments. The samples were sputtered with a 1.5 keV Ar⁺ at normal incidence. The topography images measured with AFM showed that the surface becomes smoother for the first 10 minutes of sputtering while it becomes rougher for sputtering of 30 minutes and more. The kurtosis and skewness of the topographies indicate a shift in symmetry of the height distribution. No ripple formation is observed in any of these samples. In addition the height-height correlation function was calculated from the AFM images indicating that the surfaces show a roughness with self-affine properties.

With AFM force spectroscopy force-distance experiments were performed in order to measure the adhesion force. From these experiments an inverse proportional relation to the rms roughness is found. In detail the adhesion increases for the smooth surfaces and decreases for the rougher with the lowest value to be at the 60 minutes sample. The contact angle measurements show a hydrophobic surface with a surface energy independent of the sputtering time. The four probe resistivity measurements show an increase trend proportional to the sputtering time was observed indicating the larger scattering of the electrons in the surface. Note that in this case the actual roughness is not the important parameter, but the sputter time. In general we conclude that the sputtering shifts the surface morphology with influence in roughness, adhesion and resistance.

As future perspectives there are a lot of new ideas that came out during this study. As future research the same series of experiments could be done for different time sputtering, angle of incidence and ion energy. In addition the adhesion could be measured with other AFM methods as the thermal noise excitation of the cantilever. Also X-Ray Photoelectron Spectroscopy and X-Ray Standing Wave experiments can be used in order to understand how sputtering affects the stoichiometry in the surface region.

Acknowledgments

A lot of people helped finish my thesis. Some of them currently are doing different things in different places on the planet but I feel the need to thank them all.

Thank You:

Professor Dr. Ir. Harold Zandvliet: for the support, the multitasking help and for the inspiration.

Dr. Ir. Herbert Wormeester: for all the help and guidance in the whole thesis procedure and for the freedom to do whatever I want in the lab.

Dr. Arzu Colak: for all the methodology and instrumentation help, without you there would be no thesis for me. I wish you good luck and to be happy.

Dr. Ir. Annemarie Huijser: for being the external member of my exam committee. I hope you liked my thesis.

Professor Dr. Ir. Bene Poelsema, Dr. Stefan Kooij, Dipl.-Ing. Dr. Gregor Hlawacek, Dr. Raoul van Gastel: for all the help, the advices and the fun.

In advance I want to thank the people from the PIN group and the University in general that made my days more interesting and funny:

Rik Akse: for proposing me PIN group.

Adil, Pantelis, Hasan and Huseyin: for all the help.

Hairong, Robin and Erik: for all the help with the AFM, sorry for the questioning bombardment.

Patrick: for all the help with the contact angle method, good luck with the cat.

Cora and Sander: for all the help with the four probe method and the lab access.

Kai: for the advices, you scream like Greek.

Hans and Herman: for all the help with the instrumentation, you are the best.

Simone and Jeroen: for the help with the bureaucracy.

Vasilisa, Maciej, Iris, Norah, Makis, Avijit, Rene, Chris, Tijs, Lijie: for all the happy moments during my time with you, keep up.

Imtiaz and Ali: the craziest office in the whole carre building

Last but not least I want to thank my family for all the support and of course my friends in the whole planet. Peace and much love to all of you!

Bibliography

- [1] H.-J. Butt et al. / Surface Science Reports 59 (2005) 1–152
- [2] A. S. Botana, V. Pardo, D. Baldomir, and P. Blaha, “Conducting states caused by a surface electric dipole in CrN(001) very thin films,” Phys. Rev. B, vol. 87, no. 7, p. 075114, Feb. 2013
- [3] F. Esaka, “Comparison of surface oxidation of titanium nitride and chromium nitride films studied by x-ray absorption and photoelectron spectroscopy,” J. Vac. Sci. Technol. A Vacuum, Surfaces, Film., vol. 15, no. 5, p. 2521, Sep. 1997.
- [4] Greenwood Norman, Earnshaw, Alan (1984). Chemistry of the elements, Oxford
- [5] W. R. Grove, “On the Electro-Chemical Polarity of Gases,” Philos. Trans. R. Soc. London, vol. 142, no. January, pp. 87–101, Jan. 1852.
- [6] Giannuzzi, L.A., Stevie, F.A., "Introduction to focused ion beams: instrumentation, theory, techniques, and practice", Springer (2005)
- [7] A. Herwadkar and W. Lambrecht, “Electronic structure of CrN: A borderline Mott insulator,” Phys. Rev. B, vol. 79, no. 3, p. 035125, Jan. 2009.
- [8] R. Smith, ed. (1997). Atomic & ion collisions in solids and at surfaces: theory, simulation and applications, Cambridge university press
- [9] Peter Sigmund, Theory of Sputtering. I. Sputtering Yield of Amorphous and Polycrystalline Targets, Phys. Rev. 184, 383, (1969)
- [10] S. Habenicht, K. Lieb, J. Koch, and a. Wieck, “Ripple propagation and velocity dispersion on ion-beam-eroded silicon surfaces,” Phys. Rev. B, vol. 65, no. 11, p. 115327, Mar. 2002.
- [11] G. Binnig and C. F. Quate , AFM, Phys. Rev. Lett. 56, 930–933 (1986)
- [12] Amplitude Modulation Atomic Force Microscopy, Ricardo Garcia, Wiley-VCH
- [13] Y. Zhao, G.-C. Wang and T.-M. Lu, Characterization of Amorphous and Crystalline Rough Surface (Elsevier, 2001) (ISBN 012475984X)
- [14] G. Palasantzas, A study of (1+1)-Dimensional height height correlation functions for self affine fractal morphologies, PII: S0038-1098(96)00487-5, Solid State Communications, Vol. 100, No. 10, pp. 705-710, 1996

- [15] S. K. Sinha et al., X-Ray and neutron scattering from rough surfaces, *Physical Review B*, Volume 38, Number 4, 1988
- [16] J. N. Israelachvili - Intermolecular and surface forces (1992), ISBN-10: 0123919274
- [17] J. C. Berg, An introduction to colloids and interfaces, World Scientific (November 18, 2009), ISBN-10: 9814299820
- [20] A. D. Slattery, A. J. Blanch, J. S. Quinton, and C. T. Gibson, "Accurate measurement of Atomic Force Microscope cantilever deflection excluding tip-surface contact with application to force calibration.," *Ultramicroscopy*, vol. 131, pp. 46–55, Aug. 2013
- [21] H. R. Fischer and E. R. M. Gelinck, "Determination of adhesion forces between smooth and structured solids," *Appl. Surf. Sci.*, vol. 258, no. 22, pp. 9011–9017, Sep. 2012.
- [22] Arzu Colac, Measuring Adhesion Forces Between Hydrophilic Surfaces with Atomic Force Microscopy Using Flat Tips, 2013, ISBN 978-90-365-1612-9, Physics of Interfaces and Nanomaterials group, University of Twente, 2013
- [23] Y. Rabinovich, J. Adler, a Ata, R. Singh, and B. Moudgil, "Adhesion between Nanoscale Rough Surfaces.," *J. Colloid Interface Sci.*, vol. 232, no. 1, pp. 17–24, Dec. 2000
- [24] D. Packham, "Surface energy, surface topography and adhesion," *Int. J. Adhes. Adhes.*, vol. 23, no. 6, pp. 437–448, Jan. 2003.
- [25] Pierre-Gilles de Gennes, Francoise Brochard-Wyart, David Quere, *Capillarity and Wetting Phenomena: Drops, Bubbles, Pearls, Waves*
- [26] A. Marmur, *Soft contact: Measurement and interpretation of contact angles*, The Royal Society of Chemistry, 2006, *Soft Matter*, 2006, 2, 12-17, www.rsc.org/softmatter
- [27] V. Timoshevskii, Y. Ke, H. Guo, and D. Gall, "The influence of surface roughness on electrical conductance of thin Cu films: An ab initio study," *J. Appl. Phys.*, vol. 103, no. 11, p. 113705, 2008.
- [28] C. Kittel, *Introduction to Solid State Physics*, Wiley; 8 edition (November 11, 2004), ISBN-10: 047141526X

[29] A. Çolak, H. Wormeester, H. J. W. Zandvliet, and B. Poelsema, "Surface adhesion and its dependence on surface roughness and humidity measured with a flat tip," *Appl. Surf. Sci.*, vol. 258, no. 18, pp. 6938–6942, Jul. 2012.

[30] Motoki Obata et al. Contact property between metal and tantalum nitride film characterized by using transmission line model, *Surface and Coatings Technology* 180 – 181 (2004)136–139